periodica polytechnica

Civil Engineering
55/2 (2011) 137–146
doi: 10.3311/pp.ci.2011-2.06
web: http://www.pp.bme.hu/ci

RESEARCH ARTICLE

Numerical simulation of the flutter performance of different generic bridge cross sections

Gergely Szabó / *József* Györgyi

Received 2011-03-03, accepted 2011-03-29

Abstract

This paper presents the results of numerical simulation of the flutter performance of different generic bridge cross sections. The bridge flutter assessment has become a major concern in bridge design practice. In the early ages, wind tunnel tests were made in order to assess the aerodynamic performance of bridges. In this paper the flutter performance of different bridge deck sections was investigated by using numerical flow simulation. The detailed comparison of the aerodynamic behaviour of the different cross sections in terms of flutter instability gives the engineers good means to design of bridge structures.

Keywords

Bridge deck flutter · aeroelasticity · critical wind speed

Acknowledgement

The authors are grateful for the support of the Department of Fluid Mechanics (University of Technology and Economics, Budapest), CFD.hu Ltd., Pont-TERV Ltd. and the INNOCSEKK foundation (NKTH, Hungary).

Gergely Szabó

Budapest University of Technology and Economics, Department of Structural Mechanics, H-1111 Budapest, Műegyetem rkp 3, Hungary
e-mail: mr.gergely.szabo@gmail.com

József Györgyi

Budapest University of Technology and Economics, Department of Structural Mechanics, H-1111 Budapest, Műegyetem rkp 3, Hungary
e-mail: gyorgyi@ep-mech.me.bme.hu

1 Introduction

Nowadays, with a strong computational background, CFD (Computational Fluid Dynamics) simulations appear to be powerful rivals of the wind tunnel tests [2, 4, 6, 8]. Recently a number of numerical simulations have been made in order to assess the aeroelastic behaviour of bridge structures. The most advanced ones take into account the three-dimensional motion of a bridge deck in fluid flow [5, 22]. This approach is rare nowadays, mainly because it is computationally intensive. Instead, only a two-dimensional section is considered of the bridge in CFD simulations. Many of them deal with the classical benchmark tests case; the oscillating flat plate in uniform airflow. This case is very important, because analytical solution is available to compare with. There are results for generic cross sections as well [12, 17]. In a CFD solution, the most commonly used approach is the forced vibration method. During such an analysis, the investigated cross section is oscillated with a desired harmonic motion according to either vertical or rotational degrees of freedoms. The main advantage of the forced vibration method is that the flutter derivatives can be easily extracted from the force and moment signals obtained from the simulation.

In this paper the above mentioned approach is used by utilizing the 6.3.26 version of the FLUENT commercial software [1]. Before applying it to an arbitrary bridge deck section, it was tested on generic cross sections. For this purpose a streamlined and three non-streamlined cross sections were considered that can be found in [21]. The comparison of the results will be presented.

The generic cross sections are idealized forms of real bridges and do not comprise additional elements such as curbs, barriers, handrails or even a vehicle that can alter the aerodynamic behaviour significantly. On top of all, the role of the angle of attack of the wind direction can be also important [4]. To assess the effects of the above, a real boxed bridge cross section was studied. The flutter derivatives were calculated for the bridge with and without the mentioned complementary elements at different angle of wind attack. A detailed comparison will be addressed in order to express the effects of the certain elements.

The effects of inflow turbulence are not discussed here, uni-

form airflow is assumed only. The ways of taking turbulence into account can be seen in [9, 11, 15, 16]. These pieces of work basically use offers by standards or wind tunnel measurements. There are methods, however, that might be used to determine the time dependent wind structure onto a certain terrain [14]. Such methods may be used in the near future combined with structural vibration related simulations.

2 Mathematical background

In this chapter the main mathematical formulations are presented. The first step in a flutter study should be setting up the structural dynamics model of the bridge to be analysed. In [3, 7] a detailed description can be found. If the FEM model is made, a representative section of the whole bridge deck needs to be taken. The final aim is a two degree of freedom oscillator model that can be further studied in terms of flutter instability.

2.1 Theory of the flutter derivatives

The above mentioned 2DOF system has a load vector that contains two load components. In wind tunnel tests as well as in CFD simulations the Scanlan flutter derivatives give an easy understanding of the acting forces [18, 19, 21]. In equations (1) and (2) the meaning of these derivatives are shown.

$$L(t) = \frac{1}{2}\rho U^2 B\left[KH_1^*(K)\frac{\dot{h}(t)}{U} + KH_2^*(K)\frac{B\dot{\alpha}(t)}{U} + K^2H_3^*(K)\alpha(t) + K^2H_4^*(K)\frac{h(t)}{B}\right] \tag{1}$$

$$M(t) = \frac{1}{2}\rho U^2 B^2\left[KA_1^*(K)\frac{\dot{h}(t)}{U} + KA_2^*(K)\frac{B\dot{\alpha}(t)}{U} + K^2A_3^*(K)\alpha(t) + K^2A_4^*(K)\frac{h(t)}{B}\right] \tag{2}$$

In (1), (2) L and M are the lift force and moment respectively. B is the width of the bridge deck, U is the inflow velocity, ρ is the air density, h and α are the vertical and rotational motions respectively, ω is the oscillating frequency. $K = B \cdot \omega / U$ is the reduced frequency. It can be seen that the forces can be written as a function of the reduced frequency, the oscillating amplitudes and the $H1^* - H4^*$ and $A1^* - A4^*$ flutter derivatives. The main goal is to determine these derivatives that can be used to calculate the critical wind speed.

2.2 Basics of numerical fluid dynamics simulation

If a cross section is made undergone a forced oscillation, the flutter derivatives can be extracted. To do so, the Navier-Stokes equations along with the continuity equation need to be solved. In (3) the scalar forms of these equations are shown.

$$\begin{aligned}
&\frac{\partial v_x}{\partial t} + v_x\frac{\partial v_x}{\partial x} + v_y\frac{\partial v_x}{\partial y} + v_z\frac{\partial v_x}{\partial z} = g_x - \frac{1}{\rho}\frac{\partial p}{\partial x} + \upsilon\left(\frac{\partial^2 v_x}{\partial x^2} + \frac{\partial^2 v_x}{\partial y^2} + \frac{\partial^2 v_x}{\partial z^2}\right)\\
&\frac{\partial v_y}{\partial t} + v_x\frac{\partial v_y}{\partial x} + v_y\frac{\partial v_y}{\partial y} + v_z\frac{\partial v_y}{\partial z} = g_y - \frac{1}{\rho}\frac{\partial p}{\partial y} + \upsilon\left(\frac{\partial^2 v_y}{\partial x^2} + \frac{\partial^2 v_y}{\partial y^2} + \frac{\partial^2 v_y}{\partial z^2}\right)\\
&\frac{\partial v_z}{\partial t} + v_x\frac{\partial v_z}{\partial x} + v_y\frac{\partial v_z}{\partial y} + v_z\frac{\partial v_z}{\partial z} = g_z - \frac{1}{\rho}\frac{\partial p}{\partial z} + \upsilon\left(\frac{\partial^2 v_z}{\partial x^2} + \frac{\partial^2 v_z}{\partial y^2} + \frac{\partial^2 v_z}{\partial z^2}\right)\\
&\frac{\partial v_x}{\partial x} + \frac{\partial v_y}{\partial y} + \frac{\partial v_z}{\partial z} = 0
\end{aligned} \tag{3}$$

In (3) v_i are the three velocity components, g_i are the three gravity force components, p is the pressure, ρ is the density, υ is the viscosity.

The FLUENT software solves the integral form of the (3) equations. As the direct numerical solution is not feasible, the time averaging of the NS differential equation system is done resulting in two more unknowns in case of two-equation turbulence models. Therefore two more equations are necessary to close the equations. In the simulations the widely used RNG $k - \varepsilon$ turbulence model was applied [1].

2.3 Calculation of the critical wind velocity

In case of a 2DOF system, the (4) equation system can write the wind excitation (**M**: mass matrix, **K**: stiffness matrix, **x**: displacement vector, γ: damping parameter). Such dynamic equations are found in many other structure related problems [23]. If the solution is searched in the form of (5), (4) yields (6). In (6) the **L** matrix can be written by using the Starossek notation [2], see equations (7) and (8). Finally the (8) linear eigenvalue problem is to be solved ($U_{\text{red}} = U/(B \cdot f)$, reduced velocity).

$$\mathbf{M}\ddot{\mathbf{x}} + \frac{\gamma}{\omega}\mathbf{K}\dot{\mathbf{x}} + \mathbf{K}\mathbf{x} = \mathbf{q} \tag{4}$$

$$\mathbf{x} = \tilde{\mathbf{x}}e^{i\omega t} \tag{5}$$

$$-\omega^2\mathbf{M}\tilde{\mathbf{x}} + (1 + i\gamma)\mathbf{K}\tilde{\mathbf{x}} = \omega^2\mathbf{L}\tilde{\mathbf{x}} \tag{6}$$

$$\mathbf{L} = \pi\rho b^2\begin{bmatrix} c_{hh} & c_{h\alpha} \\ c_{\alpha h} & c_{\alpha\alpha} \end{bmatrix} \tag{7}$$

$$\begin{aligned}
c_{hh} &= \frac{2}{\pi}H_4^* + i\frac{2}{\pi}H_1^*, \quad c_{h\alpha} = \frac{4}{\pi}A_4^* + i\frac{4}{\pi}A_1^*,\\
c_{\alpha\alpha} &= \frac{4}{\pi}H_3^* + i\frac{4}{\pi}H_2^*, \quad c_{\alpha\alpha} = \frac{8}{\pi}A_3^* + i\frac{8}{\pi}A_2^*
\end{aligned} \tag{8}$$

$$\left|(1 + i\gamma)\mathbf{K} - \omega^2\left[\mathbf{M} + \mathbf{L}(U_{\text{red}})\right]\right| = 0 \tag{9}$$

The equation (8) can be handled easily, since it contains 2 × 2 matrices. For large systems other techniques are necessary [10]. From (8) the ω complex natural frequencies can be extracted. This frequency carries the natural frequency and the damping of the total system (that is the bridge deck in airflow). By using (9), the total logarithmic decrement of the system can be calculated. This procedure is to be done repeatedly by varying the reduced velocity until the zero damping is found that belongs to the flutter speed.

$$\delta = 2\pi \frac{Im(\omega)}{|Re(\omega)|} \tag{10}$$

3 Generic bridge deck sections

3.1 Introduction of the CFD simulation

In this chapter four different generic bridge deck sections were studied; a streamlined, two different Tacoma-like ones and a rectangle. The numerical grid around the streamlined cross section can be seen in Fig. 1. In order to investigate the effect of the grid used, two different computational grids were applied. In Fig. 1, the left picture shows a structured (mesh#1: 104018 cells), the right one an unstructured mesh (mesh#2: 38240 cells). The unstructured mesh is easy to make, but the structured is more desirable in terms of numerical convergence.

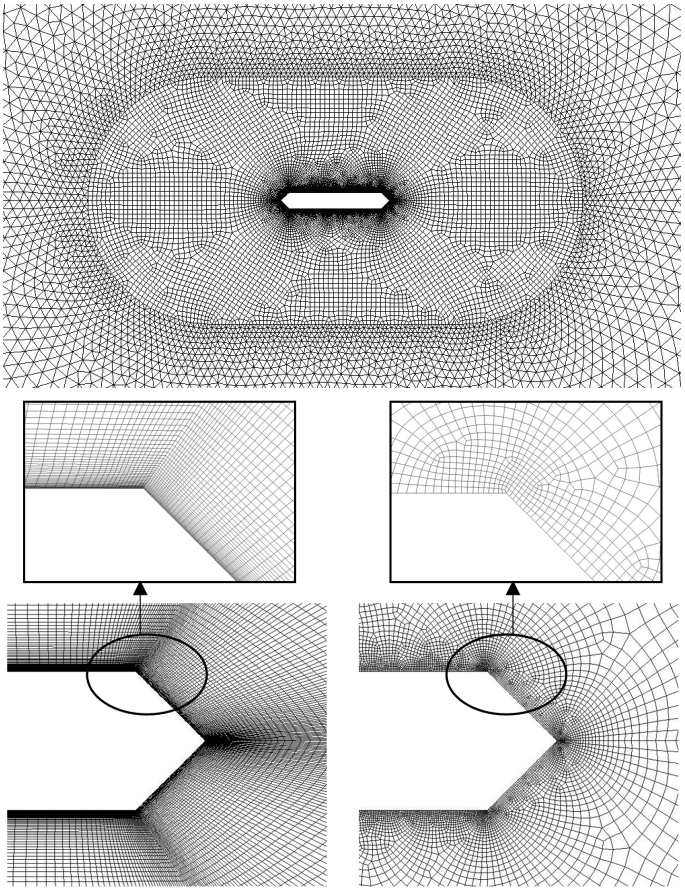

Fig. 1. Numerical grid around the streamlined cross section

In Fig. 2 the dimensions of the computational domain are shown. The boundaries of the domain are chosen to be far away from the bridge in order to decrease the effects on themselves caused by the bridge. The bridge boundary is scaled up in Fig. 2 for better visibility.

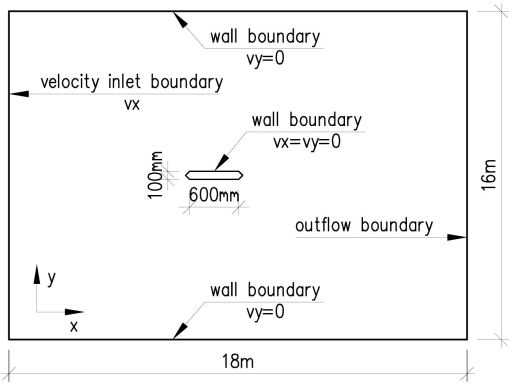

Fig. 2. Computational domain

There are many aspect of constructing a numerical grid. First of all, the number of cells needs to be as few as possible. For flutter simulation, the main goal is the determination of the flutter derivatives in (1) and (2). To do so, it is very convenient to use the forced oscillation method. During this technique, the considered bridge deck section must be given an arbitrary periodic oscillation. This oscillation is a vertical and a rotational sinusoidal motion.

As the FLUENT offers the possibility of an arbitrary function to be defined as a motion, the forced oscillation method can be easily carried out. There is a delicate issue, however, to be dealt with in detail. The motion of the bridge deck needs the reformulation of the numerical mesh around the body. There are two options to handle this problem by the software; re-meshing and mesh deformation (smoothing). The bridge suffers relatively low motion amplitude, therefore there is no need to re-mesh, and mesh deformation is enough to follow the motion. In general, the mesh in the vicinity of the bridge surface suffers great distortion, which is undesirable. To overcome this phenomenon, the mesh strategy in Fig. 1 was developed (upper picture). The main idea is that the bridge is surrounded by a rigid body mesh that does not suffer any mesh distortion and moves perfectly together with the bridge deck. In other words, the desired sinusoidal function is defined to the bridge contour and the rigid body mesh around it altogether. The rigid body mesh is made by using rectangle cells inside that are numerically advantageous as less discretization error appears. By using this technique, the good mesh quality near the bridge can be maintained. The distortion is handled by triangular cells outside that are numerically less advantageous but are really adequate to follow the motion of the rigid body mesh (see Fig. 3).

Another issue is that the mesh has to be adapted to the turbulence model chosen. As two-dimensional mesh is used, two-equation models are obvious to use. For low-Reynolds number models (e.g. SST k-ω) the y+ value in the first cell on the bridge surface is to be kept below 1. For high-Reynolds number models (e.g. RNG k-ε), the y+ value must be between 30 and 300 [1]. For the first criterion the mesh#1 fits best, for the second the

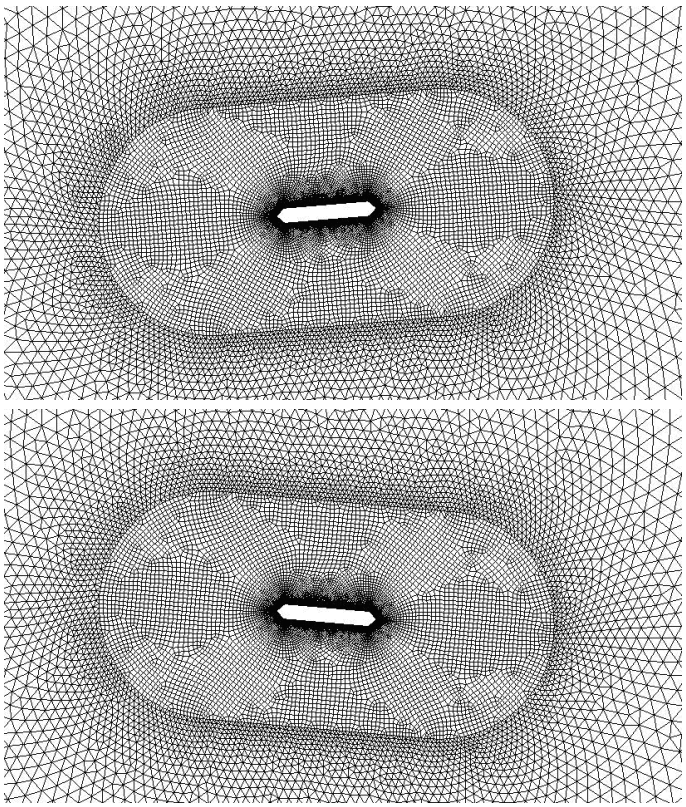

Fig. 3. Numerical grid at two different rotational states

mesh#2.

In Fig. 4 four different generic cross sections are shown. These shapes are really important to deal with as these are considered in literature [13, 17, 21]. Before calculating real bridge structures it is highly recommended to study these as benchmark cases. The above mentioned mesh#1 and mesh#2 were constructed for all these four sections.

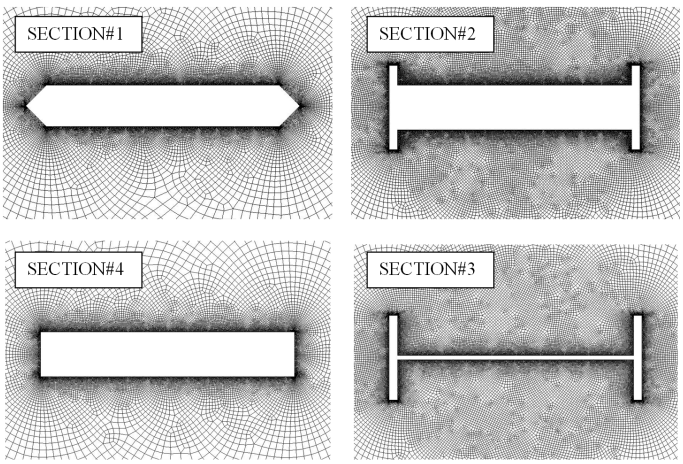

Fig. 4. Numerical grid around the four generic bridge cross sections

The streamlined cross section can be mostly approximated by using the Theodorsen theory [20]. The explanation is that the flat plate theory uses inviscid approach that is the streamlines are parallel with the oscillating body, and there is no flow separation. Numerical simulations show that though in case of SECTION#1 there is flow separation (see Fig. 6), the magnitude of that is insignificant for lower angle of attack (4^o), and the flow field even during oscillation is close to the Theodorsen theory. To be in line with this fact, the numerical grid of SECTION#1 does not need to be fine in the farther regions from the body. In case of SECTION#4 also small separation bubble is expected, though somewhat larger than in case of SECTION#1. SECTION#3 represents the highly unfavourable Tacoma cross section. The H-shape is comprised of the flat bridge deck and the stiffening girders on each side. SECTION#2 is also a model of the Tacoma cross section, but the deck width is thicker than SECTION#3. The reason for the flutter-sensitive behaviour is the large and edgy windward surface that generates high intensity vortices that roll over the bridge deck resulting in highly fluctuating wind forces [18, 19]. Over the bridge deck the shear layer is farther from the surface, therefore the mesh was consequently fine enough in these regions in order to model the high gradients in velocity and pressure accurately.

3.2 Calculation of the static force coefficients

The first step was the calculation of the static force coefficients. It is extremely important to check the numerical model and eliminate modelling errors. The force coefficients were extracted for different angle of attack from 0 to 10 by 2 degrees. SECTION#1 and SECTION#2 were investigated only. The RNG k-ε and the SST k-ω turbulence models were used on mesh#2 in each case. In Fig. 5 the calculated force coefficients are shown with respect to the angle of attack by using two different turbulence models. The average y+ value along the bridge boundary is around 8; therefore usage of the k-ε turbulence model is more correct than that of the SST k-ω. Despite this fact the results are close together except for cL at higher angle of attack values. In Fig. 6 the velocity field is shown at 4^o and 10^o angle of attacks.

In Fig. 6, it can be seen that for low angle of attack there is only a small separation bubble but for 10^o there is a large one. In Fig. 8 the velocity field is shown for SECTION#2. Even for low angle of attack there is a shear layer far away from the body. The separated flow does not reattach to the bridge deck as it can be seen in Fig. 6. In this steady simulation the importance of the mesh chosen can be understood; contrary to the findings for SECTION#1 the mesh resolution in the region of the free shear layer must be fine enough.

As a consequence of the complex geometry, the lift force turns to be positive on a certain long angle of attack range (see Fig. 7). It can be also noted that the difference between the results obtained from different turbulence models is significant for SECTION#2.

3.3 Calculation of the Strouhal number

After obtaining the static force coefficients, the unsteady behaviour was studied. To do so, an unsteady simulation was necessary. The time step selection is always a delicate issue. The smallest cell and the maximum wind speed determine the maximum time step. The so called Courant number is to be kept

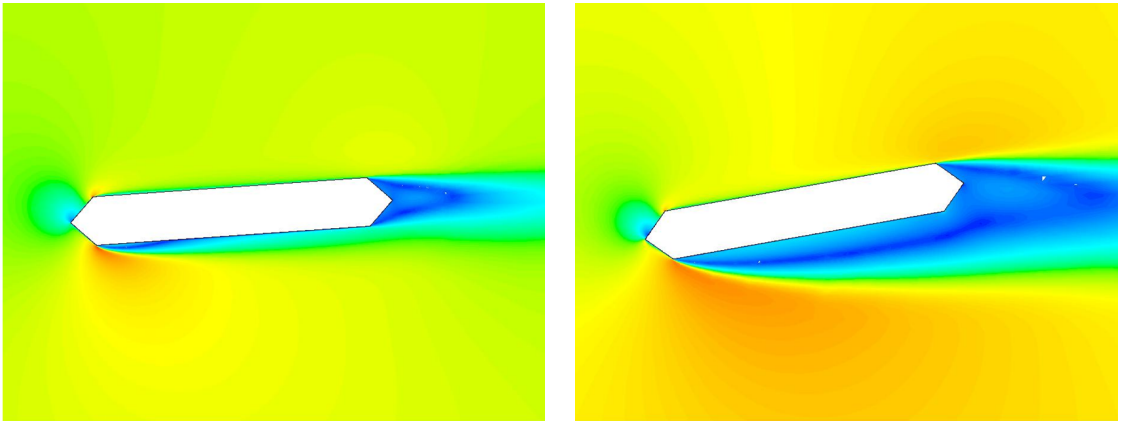

Fig. 6. Velocity magnitude contour plot for 4^o and 10^o (SECTION#1)

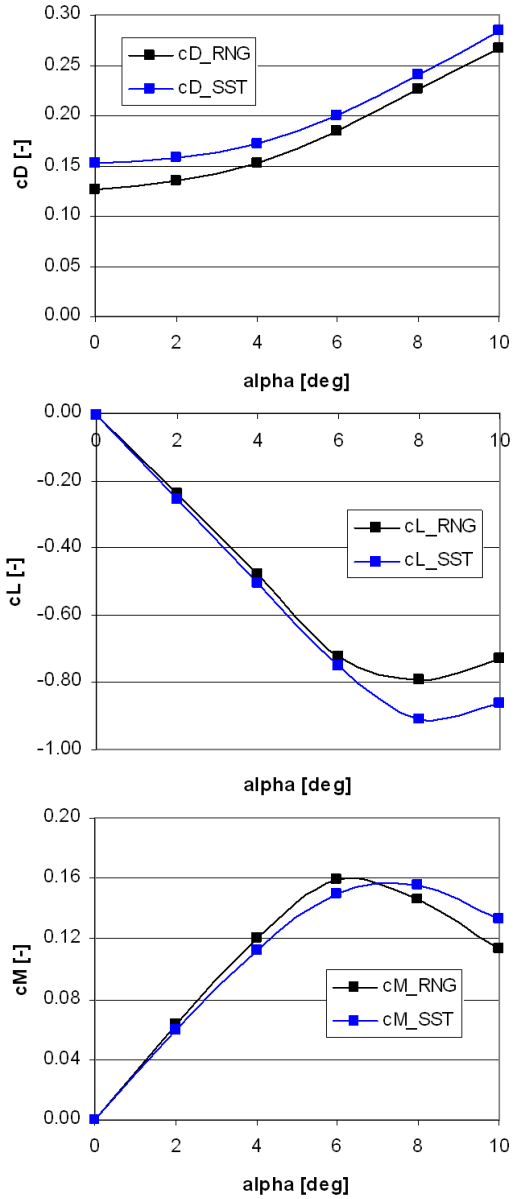

Fig. 5. Force coefficients for SECTION#1 (cD: drag, cL: lift, cM: moment)

below 1. In case of mesh#1 the time step was set to 0.00002s, while in case of mesh#2 a time step of 0.0002s was selected. In Fig. 9 the oscillating force coefficients can be seen by using the above mentioned turbulence models applied on the two different meshes providing four simulation cases. Although there are significant differences in the force amplitudes obtained from these simulations, the force frequency is almost the same for all cases. The Strouhal number was computed from the following formula:

$$Str = \frac{f \cdot D}{U} \tag{11}$$

In (10) f is the vortex shedding frequency, U is the flow speed, D is the largest crosswise dimension. The Strouhal number for SECTION#1 was 0.16. This value is close to the value of 0.17 estimated in [17]. SECTION#2 was a much tougher case in terms of capturing any oscillation. None of the mentioned turbulence models even gave unsteadiness; the oscillation was damped in the unsteady solution. The reason is that a free shear layer dominates the flow structure, and that can be only captured by using more advanced turbulence models, such as SAS (Scale Adaptive Simulation, [1]). For SECTION#2 the Strouhal number was Str=0.11 (see Fig. 10). This value is well in line with the 0.11 value calculated to a similar Tacoma-like section in [17].

In Fig. 11 and Fig. 12 the velocity magnitude contours are shown for SECTION#1 and SECTION#2 respectively. In Fig. 11 the results belonging to the RNG k-ε model can be seen. In the wake of the bridge deck the vortices are fully developed, the dynamic unsteadiness gives a sinusoidal vertically oscillating lift force to the body. The size of the wake is really small in this case and the vortex shedding happens in a well bounded region. In case of SECTION#2 (Fig. 12) the wake is really extended, and a dynamically instable shear layer oscillates around the bridge deck. To conclude, streamlined cross sections were able to be investigated by using two-equation turbulence models, while Tacoma-like sections needed SAS model to obtain reliable results.

3.4 Calculation of the flutter derivatives

For flutter calculation the most important parameters are the flutter derivatives [21]. In case of SECTION#2 a test was done in order to find the differences between the turbulence models. As it was highlighted previously, usage of RNG k-ε model is adequate to calculate vortex shedding for streamlined sections.

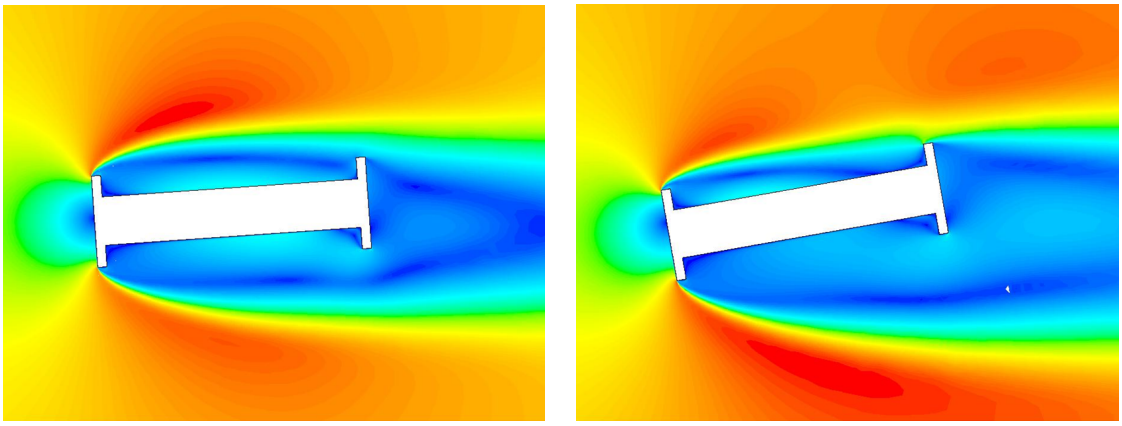

Fig. 8. Velocity magnitude contour plot for 4^o and 10^o (SECTION#2)

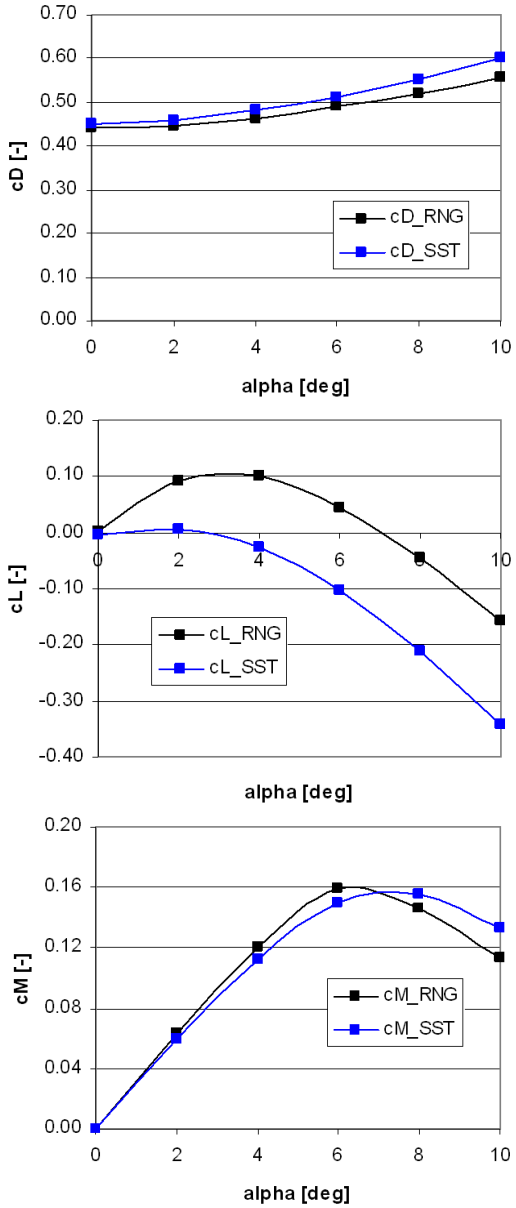

Fig. 7. Force coefficients for SECTION#2 (cD: drag, cL: lift, cM: moment)

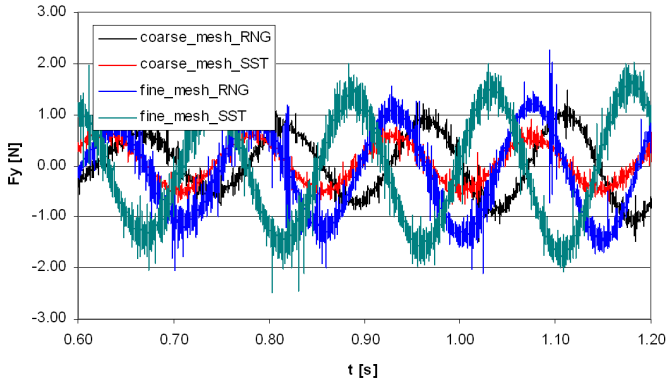

Fig. 9. Fluctuating lift force acting on the bridge deck SECTION#1

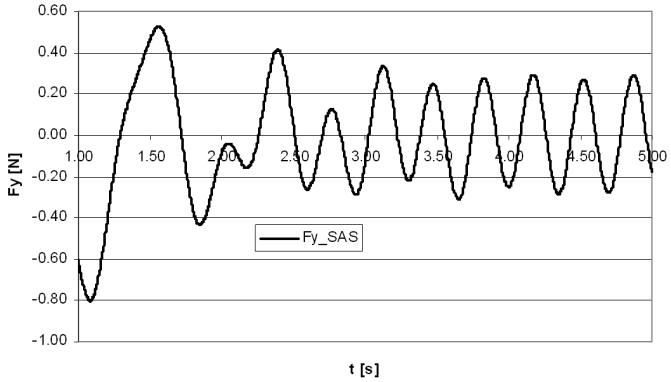

Fig. 10. Fluctuating lift force acting on the bridge deck SECTION#2

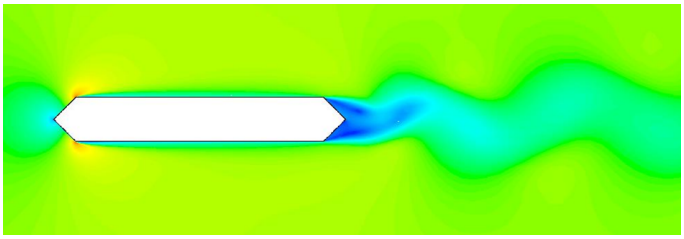

Fig. 11. Velocity magnitude contour plot for SECTION#1

At the same time, Tacoma-like sections require advanced turbulence models. As the extraction of the flutter derivatives needs unsteady simulation, it is reasonable to respect these rules. Besides, the SAS simulation needs more computational efforts and the findings for fixed bodies are not necessarily true for oscillating ones. Therefore the RNG k-ε model was used for each section even if there were significant differences between RNG k-ε and SAS models due to the fluctuations generated by the SAS model (see Fig. 13 and 14). Moreover, these differences do

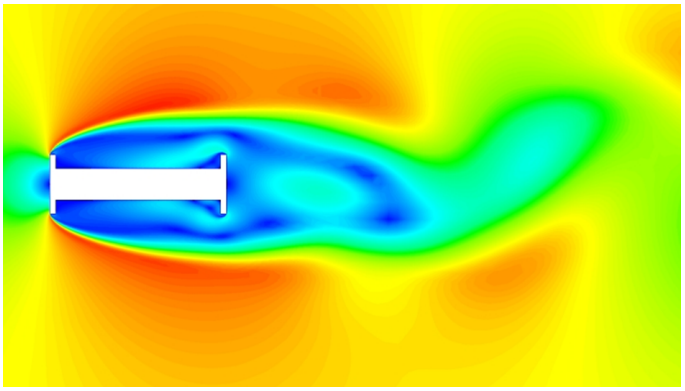

Fig. 12. Velocity magnitude contour plot for SECTION#2

not necessarily cause great differences in the calculated critical wind velocities.

Tab. 1. Reduced velocities and the belonging parameters

Ured [-]	U [m/s]	f [Hz]	α [°]	u [m]	B [m]
2.00	2.40	2.00	5.00	0.02	0.60
4.00	4.80	2.00	5.00	0.02	0.60
6.00	7.20	2.00	5.00	0.02	0.60
8.00	9.60	2.00	5.00	0.02	0.60
10.00	12.00	2.00	5.00	0.02	0.60
12.00	14.40	2.00	5.00	0.02	0.60

In Fig. 15 the velocity vector plot is shown at two different time steps by using SAS model. The unsteadiness can be clearly seen as the vortices (marked with arrows) are moving along the bridge deck. The same pattern is obtained by using the RNG k-ε model that did not provide unsteadiness on fixed bodies. In this case, however, the bridge deck is under forced oscillation that makes the flow field behave unsteady.

By performing all the simulation cases shown in Table 1 the flutter derivatives were obtained. The flutter derivatives are used to calculate the critical wind speed of a bridge deck. By analyzing the A2* derivative (see Fig. 16), important consequences can be drawn. According to (2), the A2* derivative plays an important role on the moment acting on the bridge deck in rotational oscillation. If A2* negative, there is a positive damping due to airflow. In case of an ideal flat plate, the rotational damping is always positive (see THEODORSEN in Fig. 16). This is almost the same for SECTION#1 (streamlined). SECTION#4 (rectangle) is somewhat less advantageous, because A2* tends to go positive. SECTION#2 and SECTION#3 (Tacoma sections) are prone to torsional flutter as for lower U_{red} values A2* is positive.

3.5 Calculation of the critical wind speed

After extracting the flutter derivatives the (8) eigenproblem was solved for each cross section. The critical wind speed can be determined by searching the zero-damping condition. In Fig. 17 the damping of the 2DOF system in uniform airflow is shown for the ideal flat plate SECTION#2. The delta damping values are plotted for the vertical (delta1) and rotational (delta2) motions. It is obvious that in case of the flat plate (THEODORSEN) the rotational damping turns to be zero at higher wind velocity. To the contrary, SECTION#2 behaves differently; there is a short section where the damping belonging to the vertical motion is negative causing heave-branch flutter [18]. As this happens on a shorter U_{red} section only, the torsional-branch flutter condition was also calculated.

In Fig. 18 the flutter wind speed modification factors are shown after [13]. There are many types of idealized bridge deck sections investigated in Fig. 18.

It is known that streamlined section are modified by larger factors (around 0.80 typically), that is their flutter performance is close to the flat plate. The Tacoma-like sections have a worse modification factor from 0.10 up to 0.60 as a function of side ratios and frequency ratios.

4 A specific boxed bridge deck section

Generic cross sections are really important to consider because ordinary cross sections can be idealized for practical use. The question may arise, however, how to handle a section that is not like any section contained in a standard for instance. Therefore a realistic boxed bridge deck section was considered with the usual complements (curbs, barriers and even a vehicle) that may alter the aerodynamic behaviour.

4.1 Introduction of the CFD simulation

The previously introduced generic cross sections are idealized bridge decks. The extraction of the flutter derivatives were done for those cases. In this chapter a realistic bridge deck section was investigated. The bridge shape with the numerical mesh around it can be seen in Fig. 19. The upper pictures show the bridge itself with the curbs, handrails and barriers. The lower ones represent the same bridge with an obstacle representing a lorry on the bridge either on the left or the right side of the deck.

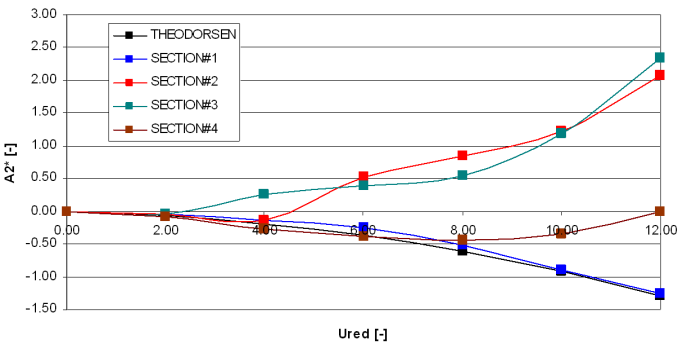

Fig. 16. A2* derivatives for the investigated cross sections

4.2 Test cases

The test cases are signed as follows; BRIDGE1: bridge in Fig. 19 (upper picture), BRIDGE2: the same bridge without curbs, handrails and barriers (this case represents a construction case), BRIDGE3: the bridge with a vehicle on the windward side, BRIDGE4: the bridge with a vehicle on the leeward

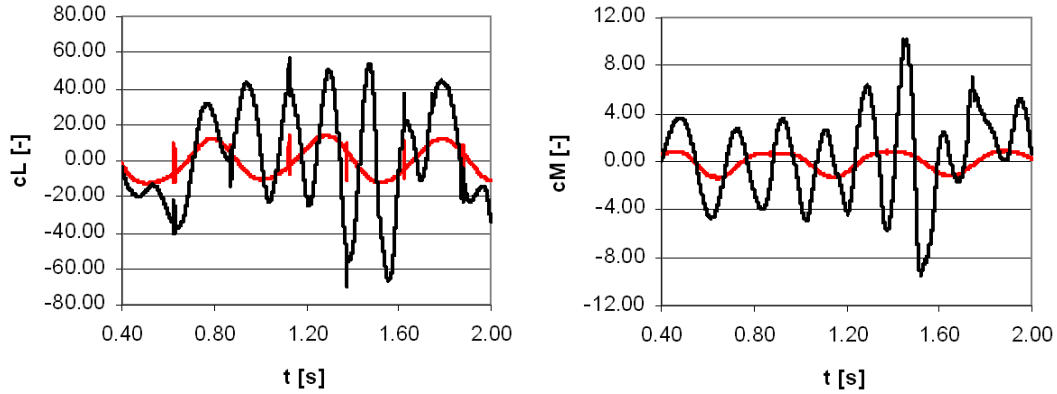

Fig. 13. Lift force and moment due to vertical motion (red: RNG k-ε, black: SAS)

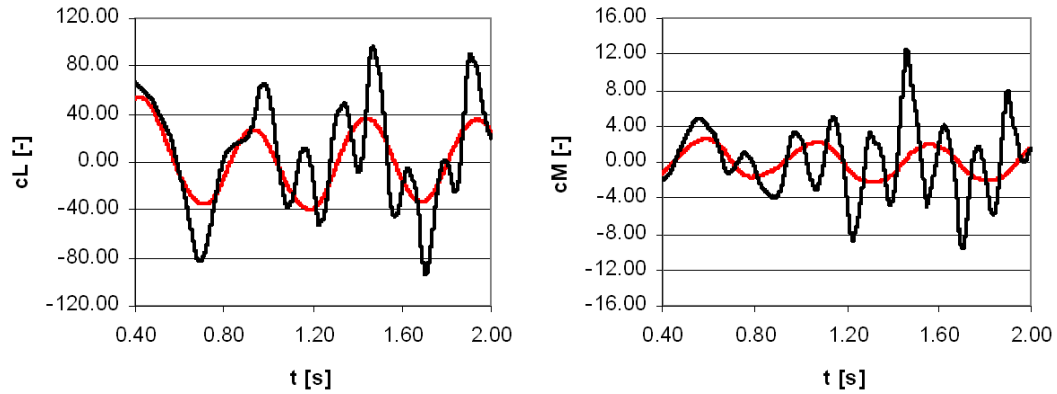

Fig. 14. Lift force and moment due to rotational motion (red: RNG k-ε, black: SAS)

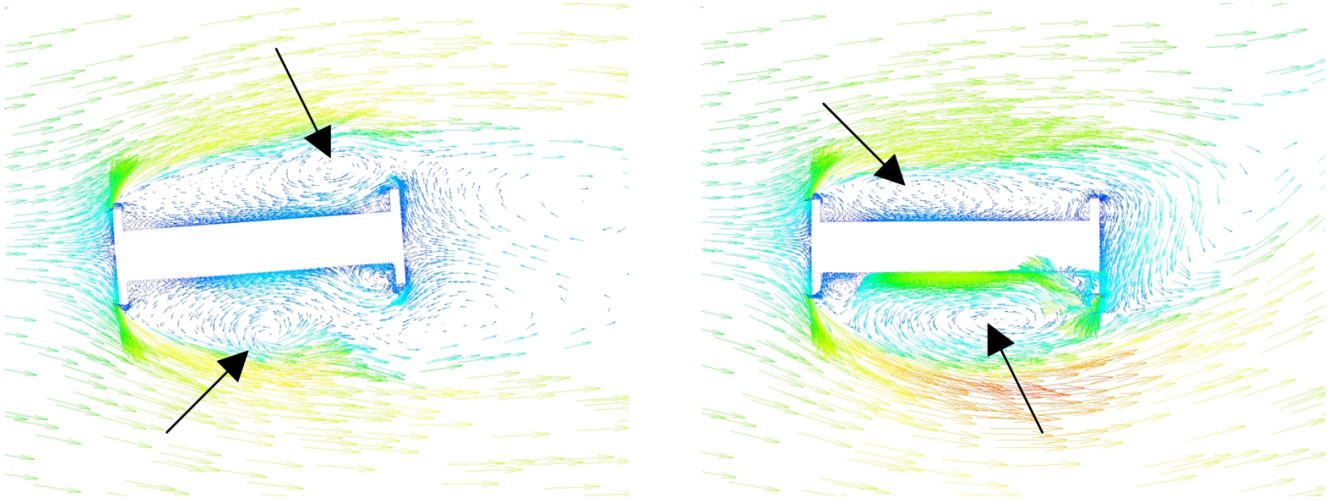

Fig. 15. Velocity vector plot by using SAS model

side. These cases were analysed by means of forced oscillation method as was used for the generic cross section. The critical wind speed modification factors were determined for all cases.

4.3 Critical wind speed

The calculated critical wind speed modification factors can be seen in Table 2. All the mentioned generic and realistic cross sections are included. BRIDGE1-4 sections are analyzed under +5, 0, -5 angle of attack of wind direction. THEODORSEN shows the analytical solution related to the ideal flat plate. The ε value indicates the ratio of the torsional and the translational frequencies. As expected, SECTION#2 (streamlined) gives a value of 0.80-0.90, well in line with the ones in Fig. 18. SECTION#4 (rectangle) shows the same behaviour. SECTION#3 (the classical Tacoma-section) produces 0.30-0.40 values. With this side ratio (d/2b=0.2) the η factor is around 0.10 according to Fig. 18 for idealized Tacoma sections. In Fig. 18, however, the real Tacoma cross section is also highlighted with a value of around 0.35, giving some confusion.

Moreover, SECTION#2 produced complex behaviour; the critical wind speed determination showed that the flutter occurs at two different wind speeds. The first wind speed belongs to the heave-branch flutter [18] (belonging to U^*_{cr}), where

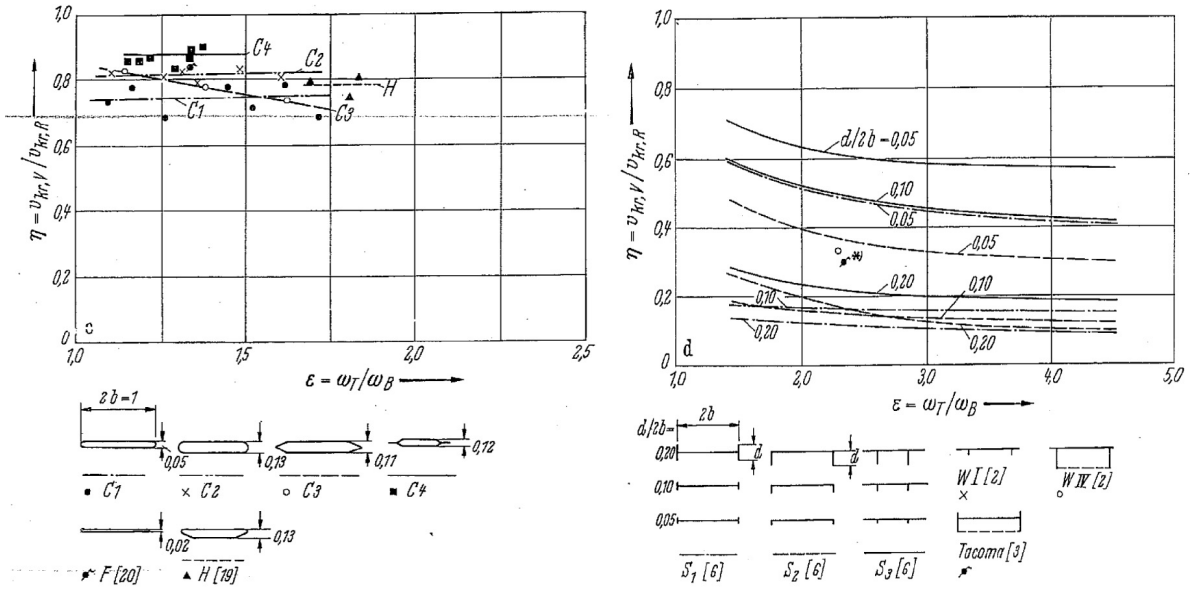

Fig. 18. Flutter wind speed modification factors

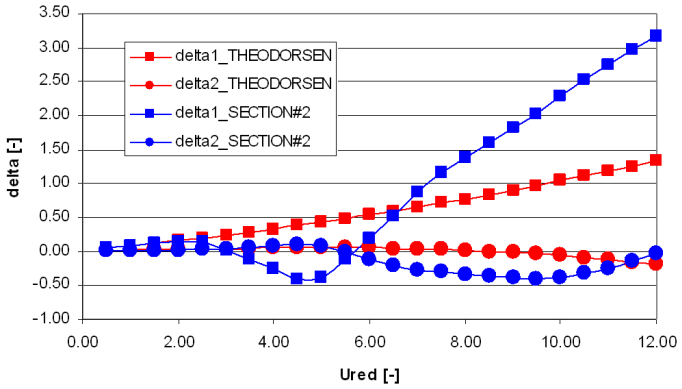

Fig. 17. Logarithmic decrement of the total system

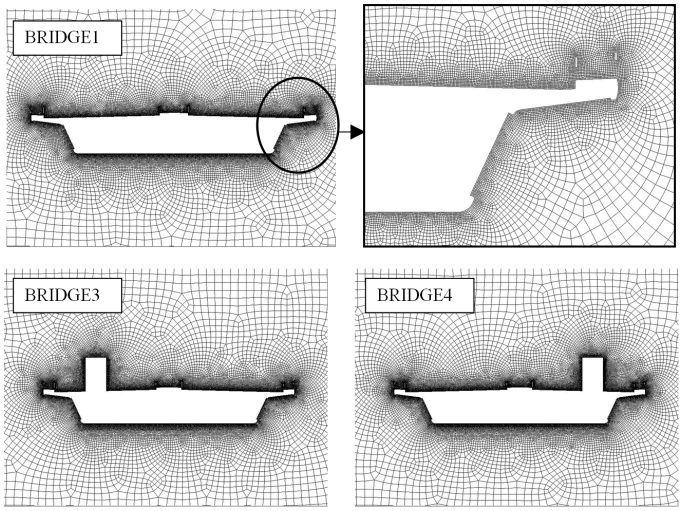

Fig. 19. Numerical mesh around the bridge section (BRIDGE2 is similar to BRIDGE1, but there are no curbs, handrails and guide rails in this case

the damping of the vertical translational frequency vanishes. With the increase of the wind speed the vertical damping goes positive again and the rotational damping vanishes, giving the classical torsional-branch flutter condition (marked with SECTION#2_m). The rotational flutter state is not so critical in this case, as the η factor is around 0.60 (belonging to U_{cr}).

Tab. 2. Critical wind speed modification factors

Ucr_α=0°												
ε	THEODORSEN		SECTION#1		SECTION#2		SECTION#2_m		SECTION#3		SECTION#4	
	Ucr	η	Ucr	η	Ucr*	η	Ucr	η	Ucr	η	Ucr	η
2	15.28	1.00	13.29	0.87	2.73	0.18	10.00	0.65	5.62	0.37	14.30	0.94
3	25.14	1.00	21.22	0.84	2.73	0.11	15.00	0.60	8.43	0.34	22.04	0.88
4	34.31	1.00	28.85	0.84	2.73	0.08	20.00	0.58	11.25	0.33	29.94	0.87
Ucr_α=+5°												
ε	BRIDGE1		BRIDGE2		BRIDGE3		BRIDGE3_m		BRIDGE4		BRIDGE4_m	
	Ucr	η	Ucr	η	Ucr*	η	Ucr	η	Ucr*	η	Ucr	η
2	15.27	1.00	16.19	1.06	2.73	0.18	9.52	0.62	2.57	0.17	10.10	0.66
3	23.06	0.92	24.99	0.99	2.74	0.11	14.25	0.57	2.57	0.10	15.10	0.60
4	30.92	0.90	33.44	0.97	2.74	0.08	18.99	0.55	2.57	0.07	19.74	0.58
Ucr_α=0°												
ε	BRIDGE1		BRIDGE2		BRIDGE3		BRIDGE3_m		BRIDGE4		BRIDGE4_m	
	Ucr	η	Ucr	η	Ucr*	η	Ucr	η	Ucr*	η	Ucr	η
2	16.60	1.09	14.83	0.97	2.39	0.16	9.46	0.62	2.50	0.16	10.06	0.66
3	24.97	0.99	23.23	0.92	2.39	0.10	14.17	0.56	2.50	0.10	14.77	0.59
4	33.33	0.97	31.65	0.92	2.39	0.07	18.88	0.55	2.50	0.07	19.67	0.57
Ucr_α=-5°												
ε	BRIDGE1		BRIDGE2		BRIDGE3		BRIDGE3_m		BRIDGE4		BRIDGE4_m	
	Ucr	η	Ucr	η	Ucr*	η	Ucr	η	Ucr*	η	Ucr	η
2	15.18	0.99	14.12	0.92	2.36	0.15	9.48	0.62	2.75	0.18	8.67	0.57
3	23.57	0.94	21.53	0.86	2.36	0.09	13.92	0.55	2.75	0.11	12.98	0.52
4	31.65	0.92	28.87	0.84	2.36	0.07	18.55	0.54	2.75	0.08	17.29	0.50

The real bridge deck section showed good performance in terms of flutter. The η factors were around 1.00 in case of construction and finished state without vehicles on it. The angle of wind attack meant noticeable differences, around ±5% with respect to the 0^o. The presence of vehicles on either side of the bridge deck alters the behaviour significantly; the heave-branch flutter rises as in case of BRIDGE3 and BRIDGE4. As mentioned there, the vertical motion damping turns to be negative on a short U_{red} section only, and the classical torsion-branch flutter shows up at higher wind speeds. The η factor belonging to the torsional flutter is around 0.60. The role of the angle of attack effect is almost the same in this case.

5 Conclusions

In this work the following conclusions were made:

- Several bridge deck sections were studied with respect to flutter instability. All the necessary parameters were calculated

by means of CFD by using the FLUENT commercial software. The static force coefficients were determined using two different turbulence models. It was shown that the streamlined cross section is not sensitive to the choice of the turbulence models but it was not the case for the Tacoma section.

- The Strouhal number was calculated easily for the streamlined section by using either of the two-equation turbulence models or meshes. The Tacoma section needed more advanced models that is adequate to model shear layer instabilities.

- The aerodynamic derivatives were extracted by using forced vibration method. A really effective meshing strategy was worked out that prevents the numerical mesh from distortion. The flutter derivatives were calculated for all the generic cross sections. Compared with data in literature good agreement was found for the streamlined section. In case of the Tacoma-like sections there were discrepancies both in literature and the numerical results as well. The critical wind speed modification factors were given in a range from 0.10-0.60. The numerical simulation showed that there could be two different types of flutter instability; heave-branch and torsional-branch flutter can occur. It was also shown that the choice of turbulence models could mean significant differences in the forces during the forced oscillation method.

- The flutter performance was determined for a real bridge cross section. The bridge section showed good behaviour in terms of flutter. The effect of the angle of attack of the wind was noticeable but not significant. The presence of large vehicles altered the aerodynamic performance; the heave-branch flutter showed up as in case of the Tacoma section. With the increase of the critical wind speed, however, the torsional flutter developed, giving a modification factor of 0.60.

- To conclude, there is a need for wind tunnel tests in order to clarify the above mentioned uncertainties; it is very important to explore that whether the heave-branch flutter even develops. The static force coefficients and the Strouhal-number will be also validated.

References

1 *Ansys Help, Release 11.0 Documentation for ANSYS*, ANSYS Inc., 2007.

2 **Avsar Ö**, *Determination of Flutter Derivatives from Free Vibration Test Results*, Master thesis, Hamburg University of Technology, 2003.

3 **Bathe K J, Wilson E L**, *Numerical methods in finite element analysis*, Prentice Hall, 1976.

4 **Brownjohn J M W, Choi C C**, *Wind tunnel section model study of aeroelastic performance for Ting Kau Bridge Deck*, Wind and Structures **4** (2001), 1–16.

5 **Cavagna L, Quaranta G, Mantegazza P**, *Application of Navier-Stokes simulations for aeroelastic stability assessment in transonic regime*, Computers and Structures **85** (2007), 818–832, DOI 10.1016/j.compstruc.2007.01.005.

6 **Chen X, Kareem A**, *Aeroelastic Analysis of Bridges: Effects of Turbulence and Aerodynamic Nonlinearities*, Journal of Engineering Mechanics **129** (2003), 885–895, DOI 10.1061/(ASCE)0733-9399(2003)129:8(885).

7 **Cheng S H, Lau D T, Cheung M S**, *Comparison of numerical techniques for 3D flutter analysis of cable-stayed bridges*, Computers and Structures **81** (2003), 2811–2822.

8 **Gu M, Qin X**, *Direct identification of flutter derivatives and aerodynamic admittances of bridge decks*, Engineering Structures **26** (2004), 2161–2172, DOI 10.1016/j.engstruct.2004.07.015.

9 **Györgyi J, Szabó G**, *Dynamic analysis of wind effects by using an artificial wind function*, Slovak Journal of Civil Engineering **3** (2008), 21–33.

10 **Györgyi J**, *Calculation of circular frequency by subspace-iteration in case of frequency-dependent dynamical stiffness matrix*, Periodica Polytechnica **33** (1989), 123–130.

11 **Hubová O**, *Wind actions on bridges*, Conference on New Trends in Statics and Dynamics of Buildings, 2007, pp. 329–330.

12 **Hübner B, Walhorn E, Dinkler D**, *Numerical Investigations to Bridge Aeroelasticity*, Fifth World Congress on Computational Mechanics, 2002, pp. 1–15.

13 **Klöppel K, Thiele F**, *Modellversuche im Windkanal zur Bemessung von Brücken gegen die Gefahr winderregter Schwingungen*, Der Stahlbau **32** (1967), 353–365.

14 **Kristóf G, Rácz N, Balogh M**, *Adaptation of Pressure Based CFD Solvers for Mesoscale Atmospheric Problems*, Boundary-Layer Meteorol **131** (2008), 85–103, DOI 10.1007/s10546-008-9325-7.

15 **Králik J, Králik J, Dinkler D**, *Deterministic and probability analysis of the steel chimney under wind loads*, 17th International Conference on Engineering Mechanics, 2011, pp. 311–314.

16 **Lajos T, Balczó M, Goricsán I, Kovács T, Régent P, Sebestyén P**, *Prediction of wind load acting on telecommunication masts*, IABSE Symposium on Responding to Tomorrow's Challenges in Structural Engineering, 2006, pp. 1–8.

17 **Larsen A, Walther J H**, *Discrete vortex simulation of flow around five generic bridge deck sections*, J. Wind Engng. And Industrial Aerodynamics **77-78** (1998), 591–602.

18 **Matsumoto M**, *International advanced school on "Wind-excited and aeroelastic vibrations of flutter"*, Department of Structural and Geotechnical Engineering University of Genova, 2000.

19 **Miyata T**, *Historical view of long-span bridge aerodynamics*, Journal of Wind Engineering and Industrial Aerodynamics **91** (2003), 1393–1410.

20 **Theodorsen T**, *General theory of aerodynamic instability and the mechanism of flutter*, National Advisory Committee for Aeronautics **496** (1935), 413–433.

21 **Scanlan R H, Tomko J J**, *Airfoil and bridge deck flutter derivatives*, Journal of Engineering Mechanics **97** (1971), 1717–1737.

22 **Szabó G, Kristóf G**, *Three-dimensional numerical flutter simulation*, The Fifth International Symposium on Computational Wind Engineering, 2010, pp. 1–8.

23 **Szőke D, Lógó J, Merzel B D**, *Optimal suspension settings for ride comfort of road vehicles*, Periodica Polytechnica **54/2** (2008), 73–78, DOI 10.3311/pp.ci.2010-2.01.